Fault Location in Transmission Systems with Large Scale Inverter-Based Resource (IBR) Integration: Challenges and Future Trends

Raphael Reis[1], Felipe Lopes[1], Francisco Gouveia[2], Athula Rajapakse[3], Paulo Pereira Jr.[4], Antonio Teixeira Neto[1], Tomaz Silva[1]

[1]Federal University of Paraíba (UFPB)
[2]Eletrobras Chesf
[3]University of Manitoba
[4]Conprove Engenharia
Brazil

SUMMARY

The environmental issues associated with the use of fossil fuel-based sources have led the world to search for cleaner alternatives to generate electrical energy. Renewable sources have appeared as promising solutions, being interconnected to power networks worldwide. With the large-scale integration of such inverter-based resources (IBRs), new challenges to the system operation are verified due to their atypical transient responses, which impacts the performance of classical fault locators. In this paper, the challenges faced by impedance- and traveling wave (TW)-based fault location techniques due to IBR operation are addressed, highlighting the trends to deal with the unconventional IBR transient responses. To do so, EMTP fault simulations, carried out at the Power System Simulator (PS Simul) software, are applied in a 230 kV/60 Hz test system, modelled with actual parameters taken from a real Brazilian power network. Full-converter-based wind generators and their associated controls are taken into account during the studies. In each simulation, comparative analysis is carried out with the voltage and current measurements taken from both conventional power source bus and wind farm power plant terminal. From the obtained results, it is demonstrated how the estimated phasors are affected by the wind farm control dynamics, as well as how the fault-induced TW patterns are impacted by the IBR operation, especially for single-ended purposes.

KEYWORDS

Fault location, inverter-based resources, renewable sources, transmission lines.

raphael.leite@cear.ufpb.br

INTRODUCTION

With the concern about environmental issues and the continuous growth in energy demand, the use of renewable energy sources (RESs) to generate electricity have increased worldwide, with the wind farms representing one of the biggest increases in the last years [1]. In 2019, for example, the estimated power capacity of such RES was about 623 MW, reaching a value around 1.017 GW in 2023 [2]. As a result, the wind farms have become key elements in the energy supply process and in the grid operation.

On the other hand, the high penetration of such power plants into the network have led the independent system operators to explore new ways to require the wind farms support during disturbance events, such as in voltage and frequency control strategies, for example [1], [3]. However, with the integration of such inverter-based resources (IBRs) into the power grid, challenges arise in maintaining the system stability and resilience, mainly due to their intermittent behavior and the inherent low inertia [1], [3]. As a consequence, unconventional operational and control-dependent characteristics are noticed, affecting the performance of classical protective relays and fault location functions [4], [5].

Basically, in cases of short-circuit occurrences in transmission lines (TLs), the utilities need to quickly identify the fault distance in order to speed up the system restoration process and to minimize economic losses [6]. In this scenario, researches and commercially-available solutions have moved toward the development of reliable and faster fault location functionalities, by using technologies such as impedance- and travelling wave (TW)-based techniques. Their performances are well-investigated in conventional (high-inertia) power grids and their challenges are commonly reported in the literature, such as the impacts of DC decaying components, loading effects and system non-homogeneity for phasor-based approaches [6], [7], for example, as well as the presence of noise-contaminated measurements for low fault inception angles and difficulties in properly time-stamping the Global Positioning System for TW-based methods [6], [8].

Although various studies are reported about the application of different types of fault location methods in conventional networks [6-10], the analyses regarding the impacts of IBRs interconnecting TLs still demand more investigations. Essentially, most of the reported works evaluate the impacts of IBRs on some protection functions, such as on distance, directional and phase-selection elements, even proposing strategies to modify the IBR controls to improve the protection operation [4], [5], [11]. Some works have also evaluated the impacts of IBRs on the fault location performance, by using impedance- or TW-based techniques [12], [13], but they typically do not investigate in detail such impacts on the phasor estimation process neither on the fault-induced TWs, especially when single-ended methods are taken into account. Works that analyze the combination of both strategies are also scarcely reported.

As a consequence, the effects on phasor estimation and fault-induced TWs during disturbances on lines interconnected by IBRs still need further studies, and a work that join both types of techniques with detailed analysis can assist utilities and researches to clarify such aspects. As a result, a more solid understanding about such topic is provided in this paper, which is able to provide the basis for the development of future improved solutions in RESs applications. These facts are the main motivation of this work.

Therefore, to demonstrate and address the challenges faced by both impedance- and TW-based fault location applications due to IBR integration into the power network, simulated oscillographic records are considered. From the impedance-based routines, the phasors are estimated by means of fixed size data windows, whose procedures are commonly used in the field. From the TW-based perspective, the fault-induced incident and reflected surges identification are thoroughly analyzed, pointing out the challenges that may be imposed by the IBR operation and how it impacts the fault location calculation.

A Brazilian EMTP-based platform is used to carry out the fault scenarios, named as Power System Simulator (PS Simul). In each simulation, the fault point is varied, whose voltage and current measurements are taken from both convencional source side and wind farm power plant bus. Thus, the challenges faced by both impedance- and TW-based fault location methods on lines interconnected by IBRs are thoroughly analyzed in this work, in which it is addressed potential alternative strategies and future trends to assist the application of such techniques for RESs networks.

THEORETICAL BACKGROUNG

- **Impedance-Based Fault Location**

Phasor estimation procedures are one of the first steps prior to the application of impedance-based fault location algorithms. Such functionalities are typically embedded in phasor-based protective devices and fault locators. Basically, they consist in using digital filters to extract the fundamental frequency of the voltage and current signals measured at the TL ends, whose waveforms are taken as input data to the fault location techniques [6], [14]. However, during short-circuit occurrences, transients with low and high frequency components may appear superimposed to the voltage and current waveshapes, which may affect the reliable operation of phasor-based routines.

The frequency response of a classical phasor estimation technique associated with a digital mimic filter is shown in Fig. 1 [14], [15]. To present the complete response of the data acquisition system, a Butterworth-type analog anti-aliasing filter was also considered for a frequency up to 8th harmonic order (480 Hz). Such value was chosen to attend the Nyquist criteria for a typical sampling rate used in impedance-based fault locators (960 Hz) [14].

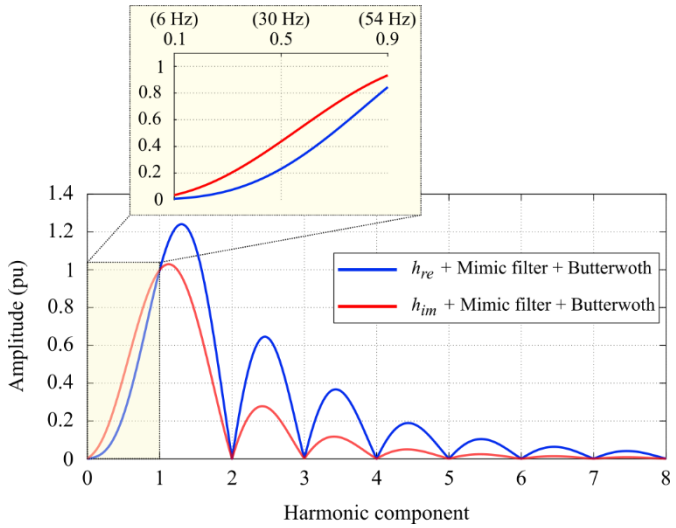

Fig. 1 – Frequency response of the combined phasor estimation technique, digital mimic and anti-aliasing filters.

As depicted in Fig. 1, the fundamental frequency of an input data is reliably estimated by the real (h_{re}) and imaginary (h_{im}) filters, providing complete attenuation of other harmonic components. Although some attenuation of inter-harmonics and subharmonics are noticed, such frequencies may still appear on the monitored voltage and current signals, impacting the proper estimation of the phasors.

The process for estimating phasors typically uses sliding data windows along the voltage and current samples, whose data window can present a fixed [14] or a variable length [16], depending on the used technique. Basically, for fixed window size strategies, the amplitude and phase of the corresponding phasors are computed with the data samples presented in the respective window (N samples/cycle) at each time step Δt. As the window slides, a new sample is added, discarding the last one. The same procedure is carried out for variable window lengths techniques, except during the short-circuit occurrence, in which the window is resized to consider only faulty data samples, minimizing the impacts of the transient period that contains both pre- and post-fault samples [16]. This data window is progressively increased up to the same size used by fixed window length routines, which takes place at the time instant when the "steady-state" fault period is reached. An illustration of the described phasor estimation process of both fixed and variable window size techniques is shown in Fig. 2.

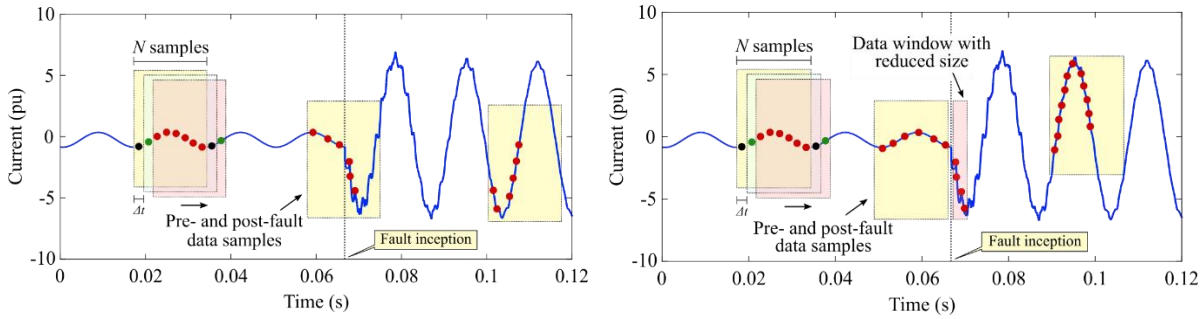

Fig. 2 – Phasor estimation process using data windows with: (a) fixed size; and (b) variable size.

As long as the voltage and current phasors are estimated, the fault location can be computed. In this paper, a classical single-ended impedance-based method is considered [17], taking into account a phasor estimation process with a fixed data window length, as commonly applied in the field. Essentially, the fault location algorithm estimates the apparent impedance between the monitored TL end and the fault point to estimate the short-circuit distance, as:

$$d = \frac{im(\hat{V}_G \cdot \Delta I_G^*)}{im(Z_{L1} \cdot \hat{I}_G \cdot \Delta I_G^*)}, \quad (1)$$

in which "im" is the imaginary part, $\hat{I}_G$ and $\hat{V}_G$ are the estimated current and voltage phasors measured at the monitored TL bus, respectively, and ΔI_G^* is the incremental current phasor. The values of $\hat{I}_G$, $\hat{V}_G$ and ΔI_G^* depend on the short-circuit type [6], [7].

- **TW-Based Fault Location**

The fundamental principle behind TW-based solutions relies on the identification of the first fault-induced surges at the monitored TL terminals [6], [8], [9]. After the short-circuit inception, TWs propagate forth and back along the TL, as illustrated in the simplified power grid shown in Fig. 3 for a short-circuit at d km away from the local bus.

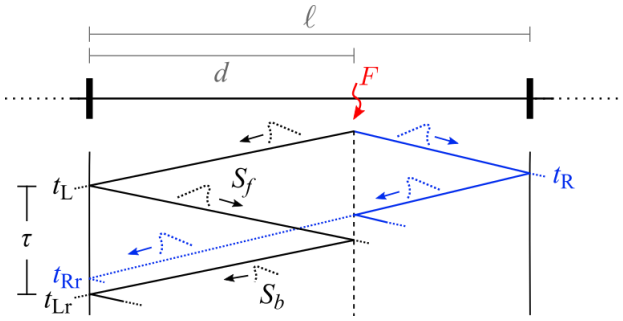

Fig. 3 – Propagation of fault-induced TWs in a simplified power grid.

Basically, single-ended TW-based fault location algorithms depend on the detection of the fault-induced incident wave, at the time instant t_L, and its correspondent reflected TW, at time t_{Lr}. This time delay τ can be used to estimate d as [6], [8]:

$$d = \frac{v \cdot \tau \cdot \Delta t}{2}, \quad (2)$$

being v the TW propagation speed.

On the other hand, double-ended TW-based approaches need the detection of the fault-induced incident TWs at both monitored TL terminals (t_L for the local bus and t_R for the remote end). Such information can be used to compute d according to [6]:

$$d = \frac{\ell + (t_L - t_R) \cdot v}{2}, \quad (3)$$

being ℓ the TL length. Here, only the single-ended approach is taken into account during the evaluations.

- **Wind Generation Unit**

In this work, full-converter-based wind generation is considered, which are typically defined as type 4. Such wind power plants consist in a mechanical turbine, a synchronous generator, a DC link and a full-converter [18]. The connection to the network at higher voltages is carried out by means of a transformer. A schematic view of the type 4 wind power unit is shown in Fig. 4.

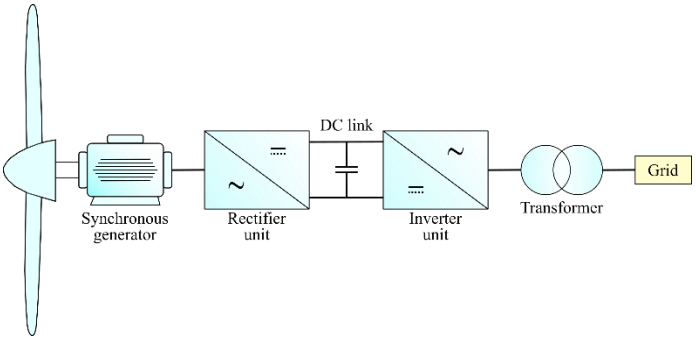

Fig. 4 – Schematic view of a type 4 wind power unit.

Basically, the turbine extracts the kinetic wind energy to be used as mechanical power by the synchronous generator, which in turn converts such power into electrical energy. In this context, the synchronous generator is uncoupled to the grid, in which a converter-based interface is used to allow such an interconnection to the network. As a result, the machine is able to operate under a variable range of speeds, producing power from variable voltage and frequency [1], [3].

The power converter-based interface consists in a rectifier unit at the synchronous generator side, and an inverter unit at the grid side. The rectifier unit converts AC voltages into DC values. In such element, different control strategies may be implemented, but they are typically designed to track the maximum power point, according to the wind conditions [1], [18]. During disturbance occurrences in the grid or overvoltages at the DC link, such control strategy can operate to reduce the energy demand, limiting the wind farm short-circuit contribution [18].

At the inverter unit side, the DC voltage is converted to AC at specified voltage and frequency. Similarly to the rectifier element, distinct control mechanisms can be used in the inverter, but they commonly control the power flow, active and reactive powers under the operating grid conditions.

TEST SYSTEM AND METHODOLOGY OF EVALUATIONS

The power network depicted in Fig. 5 was modeled using the PS Simul, which is an EMTP-type Brazilian software that allows accurate representations of electromagnetic transients and control dynamics [19]. The network consists of a 230 kV/60 Hz line 150 km long that interconnects a wind farm to the transmission grid. Step-up transformers were taken into account to increase the voltage level from the wind power plant side to the Thevenin equivalent bus, which represents the power network. The TLs were modeled as fully transposed lines using a frequency-dependent model. All the parameters of the evaluated test system were adjusted from a real Brazilian network. Besides, full-converter-based wind generators were also considered, representing in detail nonlinear elements and their associated controls [11]. Busbar and transformers stray capacitances of 0.1 μF were considered for the TW-based analysis, as recommended in [13]. A time step of 1 μs was used during the fault simulations.

Since the main idea relies on evaluating the impact of RESs integration on fault location techniques, an average wind speed equal to 15 m/s was taken into account without any intermittence or disturbance. The active and reactive powers supplied by the wind generators were controlled at 10 MW and 0 Mvar, respectively.

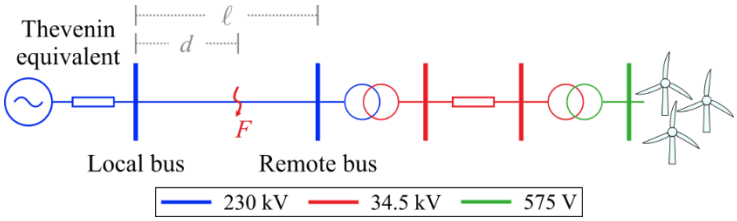

Fig. 5 – Evaluated power network

For the simulated studies, three phase short-circuits were applied at d km away from the Local bus (Thevenin equivalent side), particularly at 15 km and 135 km. The sampling rate was taken as 1 MHz for the TW-based analysis, whereas a sampling frequency of 960 Hz was considered for impedance-based functions, whose frequencies are compatible with existing practical TW- and phasor-based numerical devices. A second order low-pass Butterwoth anti-aliasing filter with cutoff frequency of 380 Hz was applied for the impedance-based application prior to estimate the voltage and current phasors, whose filters responses are shown in Fig. 1.

The fault period was set as 6 cycles to allow comparative analysis regarding the phasor-based fault location performances as a function of the number of cycles taken from the chosen voltage and current samples, although it is known that protection functions would trip in faster times. In such scenarios, the fault distances were computed by means of Eq. (1), considering up to 5 cycles after the short-circuit inception. In each simulation, the absolute error is computed as $\varepsilon = |d - \tilde{d}|$, being $\tilde{d}$ the estimated fault point.

ANALYSIS AND RESULTS

- **Simulated Records**
    - **Phasor-Based Analysis**

The PS Simul oscillographic records were used as input data for both impedance- and TW-based fault location functions. The voltage and current measurements, taken from the Local and Remote buses of the power grid presented in Fig. 5, are shown in Fig. 6 for a fault applied at 15 km away from the Local end, and in Fig. 7 for a fault taking place at 135 km. The figures at the left side are due to the Local bus, and the ones from the right side are due to the Remote bus.

From the obtained results presented in Fig. 6, even for a fault far away from the Remote bus (wind farm side), the voltage sag is quite evident in such terminal (see Fig. 6(b)), whose behavior is not similar to the one presented at the Local bus (see Fig. 6(a)). The fault current contribution from the wind farm side is significantly below from the one provided by the Local terminal (see Figs. 6(c) and (d), respectively). In fact, the Thevenin system at the Local bus represents an equivalent of a typical power system with high-inertia power plants, whose usual characteristic consists in high fault current contributions. As a result, due to the inherent feature of low-inertia and the control dynamics in limiting the short-circuit currents for the wind generation plant, the performance of the IBR technology presents atypical responses under disturbance conditions.

At steady-state, the voltage and current measurements taken from both Local and Remote buses present similar harmonic contents, as expected, which are shown in the areas 1 and 2 in Fig. 6. However, during the fault period, the voltage measured at the wind farm side presents more evident subharmonics than the ones taken from the Local end, although their amplitude are quite lower than the fundamental frequency (see Figs. 6(a) and (b)). For the current measurements, higher inter-harmonics are presented at the wind plant side, whose frequency components are not completed damped by the phasor estimation routine (vide frequency response of the system acquisition data depicted in Fig. 1), leading to some oscillations in the corresponding current phasor (see Fig. 6(d)).

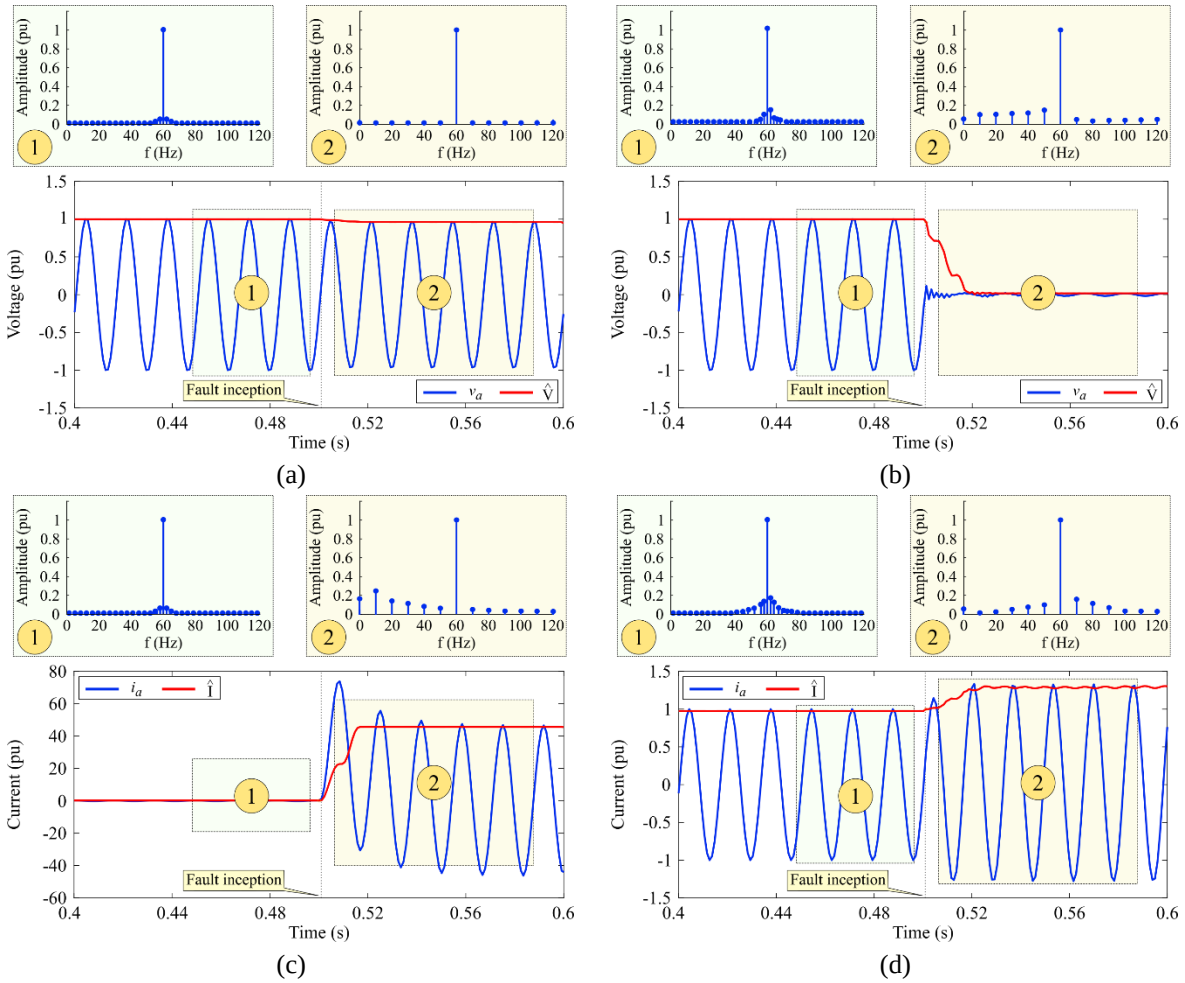

Fig. 6 – Comparative analysis about the phasor estimation process for a fault at $d = 15$ km: (a) voltage at Local bus; (b) voltage at the Remote bus; (c) current at the Local bus; and (d) current at the Remote bus.

Regarding the obtained results shown in Fig. 7 for a short-circuit at 135 km, similar analysis can be carried out as the ones for a fault at 15 km. However, the voltage signals measured at the Remote terminal present higher amplitudes of subharmonics and inter-harmonics, leading to greater oscillations in the respective estimated phasors. On the other hand, as there is a significant voltage sag during the fault period, following the wind farm control-dependent dynamics, such oscillations present themselves with low magnitudes.

The estimated fault location estimations are presented in Table I, considering both Local and Remote terminals as references to apply Eq. (1). It is worth mentioning that for a short-circuit applied at 15 km from the Local bus, the reference of the Remote end is its complement, i.e., 135 km.

From the results shown in Table I, the best estimations were obtained considering the voltage and current phasors taken from the Local bus, in which the errors decrease as the number of cycles used as input data to the fault location function increases, which is a typical performance. In fact, as the Thevenin equivalent presented at the Local end represents a conventional power source, the high fault current contributions assist in the fault location process. On the other hand, the IBR atypical fault response characteristic directly impacts the fault location performance, irrespective to the used number of cycles as input data. This characteristic is quite different from the one obtained by conventional sources. Besides, the errors can fall into a wider range than the ones expected for impedance-based techniques (in the order of 2 – 3 km [6]).

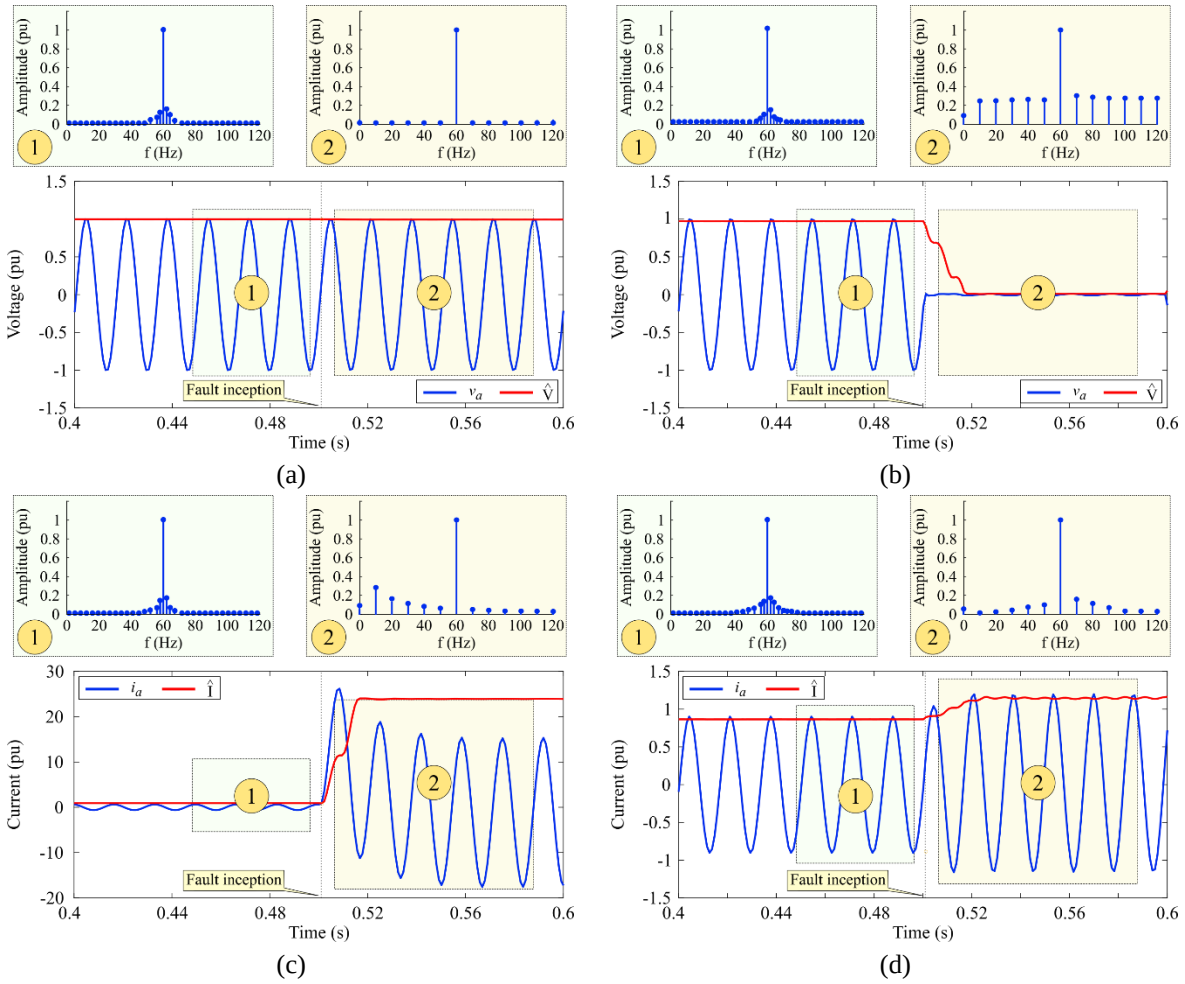

Fig. 7 – Comparative analysis about the phasor estimation process for a fault at $d = 135$ km: (a) voltage at Local bus; (b) voltage at the Remote bus; (c) current at the Local bus; and (d) current at the Remote bus.

Table I – Obtained fault location estimations for faults applied at 15 km and 135 km away from the Local bus, as a function of the number of cycles

Reference terminal	Number of cycles	$d = 15$ km		$d = 135$ km	
		$\tilde{d}$	ε (km)	$\tilde{d}$	ε (km)
Local (Thevenin equivalent)	1	15,85	0,85	135,17	0,17
	2	14,98	0,02	134,88	0,12
	3	14,98	0,02	135,17	0,17
	4	14,98	0,02	135,08	0,08
	5	14,98	0,02	135,12	0,12
Remote (wind farm plant)	1	72,52	62,48	232,3	217,3
	2	32,16	102,84	6,56	8,44
	3	82,05	52,95	6,17	8,83
	4	132,89	2,11	12,95	2,05
	5	141,51	6,51	16,64	1,64

- **TW-Based Analysis**

For the TW-based fault location analysis, the voltage and current measurements were taken in each TL monitored terminal to compute the forward and backward TW relaying signals, named as $S_{forward}$ and $S_{backward}$, respectively, which are represented as S_f and S_b in Fig. 3. Basically, such signals are correlated to each other by means of a correlation function. The maximum positive peak in its output corresponds in the time instant in which there is a best match between the fault-induced reflected and

incident surges, whose time delay is depicted as τ in Fig. 3. The τ is then used in Eq. (2) to estimate the fault distance by means of a single-ended TW-based fault locator. The technique used in this paper is reported in [8].

The TW relaying signals and the correlation function output taken from both Local and Remote ends are shown in Fig. 6 for a fault at 135 km, i.e., closer to the wind farm terminal.

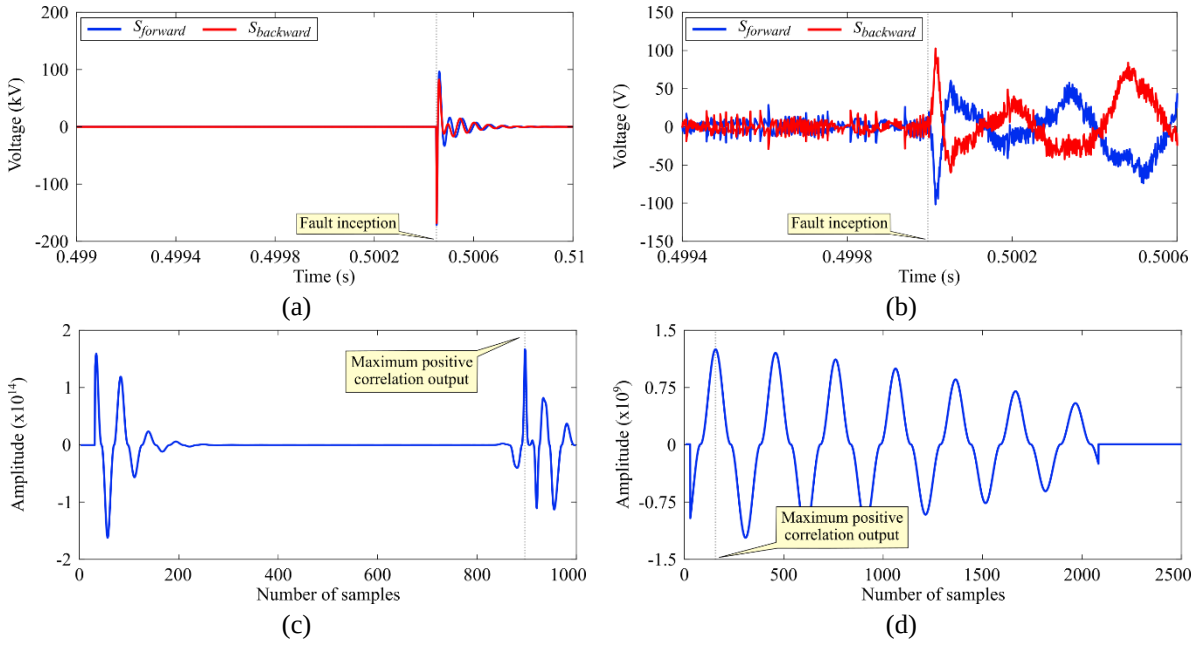

Fig. 6 – TW relaying signals for a fault at $d = 135$ km: (a) $S_{forward}$ and $S_{backward}$ at Local bus; (b) $S_{forward}$ and $S_{backward}$ at Remote bus; (c) Correlation function output at Local bus; and (d) Correlation function output at Remote bus.

Comparing the $S_{forward}$ and $S_{backward}$ signals shown in Figs. 6(a) and (b) taken from both Local and Remote buses, respectively, the waveforms measured at the wind farm generation side are more affected by its associated control dynamics, impacting, consequently, in the amplitude and transient components of $S_{forward}$ and $S_{backward}$. Differently, the corresponding signals at the Local bus present higher amplitudes and they are less affected during the steady-state operation. As a result, the correlation function output is directly impacted at the Remote end, presenting a considerable oscillatory behavior with low frequencies. Similar analysis was noticed for a fault at different points. The estimated fault location errors are presented in Table II.

Table II – Obtained TW-based fault location estimations for faults applied at 15 km and 135 km

Reference terminal	$d = 15$ km		$d = 135$ km	
	$\tilde{d}$	ε (km)	$\tilde{d}$	ε (km)
Local (Thevenin equivalent)	15,70	0,70	134,35	0,65
Remote (wind farm plant)	138,40	3,40	22,21	7,21

From the results presented in Table II, the best estimations were obtained by the measurements taken from the Local end. In fact, since the waveshapes of $S_{forward}$ and $S_{backward}$ are not affected by any atypical transient content induced by the wind farm control dynamics, the performance of the single-ended TW-based fault locator is improved, resulting in errors lower than two tower spans. On the other hand, the unusual responses of the wind generation side have led the method to misoperate, resulting in errors quite higher than the ones expected for TW-based applications (two to three tower spans). As a result, the TWs may not be reliability identified at the wind farm generation terminal, especially when the main goal is identifying the fault-induced reflected surges, as in single-terminal applications.

Therefore, both types of fault location functions experienced challenges due to the interconnection of IBRs. For the impedance-based technique, the low short-circuit current contributions and the IBR control dynamics have led the fault location function to misoperate, presenting an atypical response irrespective to the number of cycles used as input data to such routine. Similarly, for the one-ended TW-based fault location algorithm, which operates by means of a correlation function, different transient content was noticed even prior to the short-circuit application, which directly impacted the fault location performance.

As a consequence, there is a need to develop new functionalities more immune to the effects of the control dynamics and low fault currents. For impedance-based applications, for example, multi-method methodologies could be pursued, in order to select distinct fault location formulations depending on the used control strategy and the fault type. Regarding the TW-based devices, the use of them is increasing in the field, as they appear as potential solutions to speed up the protective relay performances. For fault location purposes, the identification of the fault-induced reflect surge is also challenging, as it still is for typical grids. The use of measurements taken from both TL terminals may reduce the impacts of the IBRs, since they depend on the first TW.

CONCLUSIONS

In this paper, the challenges faced by both single-ended impedance- and TW-based fault location applications due to IBR integration into the network were addressed. To do so, PS Simul (EMTP) fault simulations were applied in a transmission system interconnected by means of a wind farm power plant at the Remote bus, whose parameters were adjusted from a real Brazilian network. The nonlinear elements and the associated controls of a full-converter-based wind generators were used at the wind farm side.

From the obtained results, both of the fault location functions were affected by the unconventional operational and control-dependent characteristics of the RESs. Basically, the IBR atypical fault response characteristic impacted the impedance-based fault location performance, irrespective to the used number of cycles as input data, in which such feature is quite different from the one obtained by conventional sources. Regarding the TW-based approach, atypical transient content is induced by the wind farm control dynamics, impacting the performance of single-terminal methods in properly identifying the fault-induced reflected surges.

Therefore, some strategies could be pursued to minimize the impacts of IBR control-dependent characteristics, such as the use of multi-method methodologies depending on the used control scheme and the short-circuit type, for phasor-based solutions. For TW-based functionalities, the detection of the fault-induced reflected surges is also challenging, and the use of communication links to allow measurements taken from both TL terminals may reduce the impacts of such IBRs. In these cases, the wind farm control-dependent features have increased the complexity in properly detecting the reflected TWs, even though such task is still a challenging for conventional grids.

BIBLIOGRAPHY

[1] S. D. Ahmed, F. S. M. Al-Ismail, M. Shafiullah, F. A. Al-Sulaiman and I. M. El-Amin, "Grid Integration Challenges of Wind Energy: A Review," in *IEEE Access*, vol. 8, pp. 10857-10878, 2020, doi: 10.1109/ACCESS.2020.2964896.

[2] International Renewable Energy Agency (IRENA), Renewable energy statistics 2024, Abu Dhabi, 2024.

[3] T. Kalogiannis, E. M. Llano, B. Hoseinzadeh and F. F. da Silva, "Impact of high-level penetration of wind turbines on power system transient stability," *2015 IEEE Eindhoven PowerTech*, Eindhoven, Netherlands, 2015, pp. 1-6, doi: 10.1109/PTC.2015.7232312.

[4] A. Banaiemoqadam, A. Hooshyar and M. A. Azzouz, "A Control-Based Solution for Distance Protection of Lines Connected to Converter-Interfaced Sources During Asymmetrical Faults," in *IEEE Transactions on Power Delivery*, vol. 35, no. 3, pp. 1455-1466, June 2020, doi: 10.1109/TPWRD.2019.2946757.

[5] F. V. Lopes, M. J. B. B. Davi, M. Oleskovicz, A. Hooshyar, X. Dong and A. A. A. Neto, "Maturity Analysis of Protection Solutions for Power Systems Near Inverter-Based Resources," in *IEEE Transactions on Power Delivery (Early Access)*, doi: 10.1109/TPWRD.2024.3420421.
[6] M.M. Saha, J. Izykowski, E. Rosolowski, Fault Location on Power Networks, Vol. 2, Springer, 2010.
[7] S. Das, S. Santoso, A. Gaikwad, and M. Patel, “Impedance-based fault location in transmission networks: theory and application,” IEEE Access, vol. 2, pp. 537–557, 2014.
[8] R. Reis, F. Lopes, W. Neves, D. Fernandes Jr., C. Ribeiro, and G. Cunha, “An improved single-ended correlation-based fault location technique using traveling waves,” International Journal of Electrical Power and Energy Systems, vol. 132, p. 107167, 2021.
[9] F. V. Lopes, R. L. A. Reis, K. M. Silva, A. Martins-Britto, E. P. A. Ribeiro, C. M. Moraes, and M. A. M. Rodrigues, “Past, present, and future trends of traveling wave-based fault location solutions,” in 2021 Workshop on Communication Networks and Power Systems (WCNPS), 2021, pp. 1–6.
[10] R. L.A. Reis, W. L.A. Neves, D. Fernandes Jr., Influence of instrument transformers and anti-aliasing filters on the performance of fault locators, Electric Power Systems Research, Volume 162, 2018, Pages 142-149, ISSN 0378-7796.
[11] J. S. Costa *et al*., "Phasor-based and time-domain transmission line protection considering wind power integration," *15th International Conference on Developments in Power System Protection (DPSP 2020)*, Liverpool, UK, 2020, pp. 1-6, doi: 10.1049/cp.2020.0012.
[12] M. J.B.B. Davi, M. Oleskovicz, F. V. Lopes, An impedance-multi-method-based fault location methodology for transmission lines connected to inverter-based resources, International Journal of Electrical Power & Energy Systems, Volume 154, 2023, ISSN 0142-0615.
[13] F. V. Lopes, M. J.B.B. Davi, M. Oleskovicz, Assessment of traveling wave-based functions in inverter-based resource interconnecting lines, Electric Power Systems Research, Volume 223, 2023, 109578, ISSN 0378-7796.
[14] A. G. Phadke and J. S. Thorp, *Computer relaying for power systems*. John Wiley & Sons, 2009.
[15] BENMOUYAL, G. Removal of DC-Ofset in Current Waveforms Using Digital Mimic Filtering. IEEE Transaction on Power Delivery, v. 10, n. 2, p. 621630, Apr 1995.
[16] B. Kasztenny, M. V. Mynam, T. Joshi, and C. Daniels, “A new digital filter using window resizing for protective relay applications,” in *15th International Conference on Developments in Power System Protection (DPSP 2020)*, pp. 1–6, 2020.
[17] T. Takagi, Y. Yamakoshi, M. Yamaura, R. Kondow, and T. Matsushima, “Development of a new type fault locator using the one-terminal voltage and current data,” IEEE Transactions on Power Apparatus and Systems, vol. PAS-101, no. 8, pp. 2892 –2898, aug. 1982.
[18] Z. Chen, J. M. Guerrero, and F. Blaabjerg, “A review of the state of the art of power electronics for wind turbines,” IEEE Transactions on power electronics, vol. 24, no. 8, pp. 1859–1875, 2009.
[19] PS SIMUL: Software for Power System Modeling and Simulation of Electromagnetic Transients (in Portuguese), Conprove Engenharia, Industry and Commerce, 2019.